https://doi.org/10.5194/gmd-2022-207
Preprint. Discussion started: 7 November 2022

Geoscientific Model Development Discussions

Implementation and application of Ensemble Optimal Interpolation on an operational chemistry weather model for improving $PM_{2.5}$ and visibility predictions

Siting Li[1], Ping Wang[1], Hong Wang[1], Yue Peng[1], Zhaodong Liu[1], Wenjie Zhang[1], Hongli Liu[1], Yaqiang Wang[1], Huizheng Che[1], Xiaoye Zhang[1]

[1]State Key Laboratory of Severe Weather & Key Laboratory of Atmospheric Chemistry of CMA, Chinese Academy of Meteorological Sciences, Beijing, China

Correspondence to: Ping Wang (wangp@cma.gov.cn); Hong Wang (wangh@cma.gov.cn)

Abstract. The data assimilation technique is one of the important ways to reduce the uncertainty of atmospheric chemistry model input and improve the model forecast accuracy. In this paper, an ensemble optimal interpolation assimilation (EnOI) system for a regional online chemical weather numerical forecasting system (GRAPES_Meso5.1/CUACE) is developed for operational use and efficient updating of the initial fields of chemical components. A heavy haze episode in eastern China was selected, and the key factors affecting the EnOI, such as localization length-scale, ensemble size, and assimilation moment, were calibrated by sensitivity experiments. The impacts of assimilating ground-based $PM_{2.5}$ observations on the model chemical initial field and $PM_{2.5}$, visibility forecasts were investigated. The results show that assimilation of $PM_{2.5}$ significantly reduces the uncertainty of the initial $PM_{2.5}$ field. The mean error and root mean square error (RMSE) of initial $PM_{2.5}$ for mainland China have all decreased by more than 75%, and the correlation coefficient could be improved to more than 0.95. Even greater improvements appear in North China. For the forecast fields, assimilation of $PM_{2.5}$ improves $PM_{2.5}$ and visibility forecasts throughout the lead time window of 24 h. The $PM_{2.5}$ RMSE can be reduced by 10%-21% within 24 h, but the assimilation effect is most obvious in the first 12 h. The assimilation moment chosen at 1200 UTC is more effective than that at 0000 UTC for improving the forecast, because the discrepancy between simulation and observation at 1200 UTC is larger than that at 0000UTC, indicating the assimilation efficiency will be higher when the bias of the model is higher. Assimilation of $PM_{2.5}$ also improves visibility forecast accuracy significantly. When the $PM_{2.5}$ increment is negative, it corresponds to an increase in visibility, and when the $PM_{2.5}$ analysis increment is positive, visibility decreases. It is worth noting that the improvement of visibility forecasting by assimilating $PM_{2.5}$ is more obvious in the light pollution period than in the heavy pollution period, since visibility is much more affected by humidity during the heavy pollution period accompanied by low or extreme low visibility. To get further visibility improvement, especially for extreme low visibility during severe haze pollution, not only $PM_{2.5}$ but also relative humidity should be simultaneously assimilated as well.

https://doi.org/10.5194/gmd-2022-207
Preprint. Discussion started: 7 November 2022

Geoscientific Model Development Discussions

1 Introduction

Air pollution is an intractable problem that all developing countries with high population in the world are facing at present. The rapid development of industrialization and urbanization has led to different degrees of air pollution in many countries and regions (Perez et al., 2020; Xiao et al., 2020; Sahu and Kota, 2017). The energy-intensive and coal-fired economy in China has led to a dramatic deterioration in air quality over the past three decades(Piovani, 2017). $PM_{2.5}$ plays an important role in air pollution, and its concentration will directly affect air quality. From the health perspective, long-term exposure to high concentrations of $PM_{2.5}$ has adverse effects on the human body, including the respiratory system, cardiovascular disease and other chronic diseases(Ghorani-Azam et al., 2016); from the meteorological perspective, low visibility events occur frequently during the haze period. Aerosol particles can effectively absorb and scatter solar radiation, changing the intensity and direction of sunlight, resulting in reduced atmospheric horizontal visibility(Liu et al., 2019; Yadav et al., 2022; Ting et al., 2022), which will affect people's daily travel and traffic safety, etc.

Accurate $PM_{2.5}$ and visibility forecasts are critical for air quality assessment and public transportation safety issues(Hu et al., 2013). Chemistry Transport Model (CTM) is a key tool for $PM_{2.5}$ and visibility forecasting, and is pivotal in air quality and atmospheric chemistry research. However, various uncertainties exist in the simulation of atmospheric components in CTM, especially for aerosols(Lee et al., 2016). The complexity of atmospheric pollution formation mechanisms and model structure, the uncertainty of chemical initial conditions (ICs) and the lag in emission inventories lead to a deviation of air quality forecast results from observed comparisons, which can reach 30-50% under heavy pollution conditions(Zheng et al., 2015). The forecast accuracy of air quality forecasting still needs to be improved (Chen et al., 2016; Peng et al., 2021a).

Data assimilation (DA) is one of the most effective ways to improve model predictions. It combines observational information with numerical models to provide an estimate of the state of the system which is widely used in atmospheric, oceanic, and land surface surveys. DA were earliest applied to numerical weather prediction(Navon, 2009). There are many DA methods for example, Polynomial Interpolation(Panofsky, 1949; Gilchrist and Cressman, 1954), the methods of successive corrections(Bergthórsson and Döös, 1955), and the Kalman Filter(KF)(Kalman, 1960), the optimal interpolation (OI) (Gandin, 1963), the variational assimilation methods (e.g., the three-dimensional variational assimilation (3D-VAR), the four dimensional variational assimilation (4D-Var)) (Talagrand and Courtier, 1987; Derber, 1989), Ensemble Kalman filter method (EnKF) (Evensen, 1994), Ensemble Optimal Interpolation (EnOI) (Oke et al., 2002; Evensen, 2003) , etc. The use of data assimilation in atmospheric chemistry models to improve air quality forecasting is more recent. For example, by assimilating aerosol observations with OI(Zheng et al., 2018; Tombette et al., 2009; Carnevale et al., 2021; Tang et al., 2015; Mauricio Agudelo et al., 2015); 3D-Var(Fu and Zhu, 2011; Feng et al., 2018; Wang et al., 2020; Li et al., 2013; Liu et al., 2011; Ye et al., 2021); 4D-Var(Cao et al., 2022; Wang et al., 2021; Liu et al., 2021; Skachko et al., 2016; Zhang et al., 2011); EnKF(Lin et al., 2007; Tang et al., 2011; Pagowski and Grell, 2012; Tang et al., 2016; Lopez-Restrepo et al., 2020; Park et al., 2022); EnOI(Wang et al., 2016); Four-dimensional ensemble Kalman filter (4DEnKF)(Cheng et al., 2019)； Four-Dimensional Local Ensemble Transform Kalman Filter（4D-LETKF)(Dai et al., 2019). In OI and 3D-Var the background error covariance (BEC)

https://doi.org/10.5194/gmd-2022-207
Preprint. Discussion started: 7 November 2022


Geoscientific Model Development Discussions

matrix is estimated at once and the prediction error is statistically stationary. 4D-Var requires coding the adjoint model, which is difficult to perform for complex systems. Notably, the problem of BEC forecasting in OI and 3D-Var is solved by EnKF using a Monte Carlo approach. EnKF obtains the forecast ensemble by integrating the model multiple times and uses the empirical covariance of the forecast ensemble to update all ensemble members to obtain the analysis ensemble. When the number of ensemble members tends to infinity, the empirical covariance of the forecast ensemble approximates the true value of the forecast error covariance. Compared with variational assimilation, EnKF has a flow-dependent BEC and does not require an adjoint model, which is an advantageous data assimilation method. Several studies applied EnKF to assimilate surface or satellite observations to improve the CTM model forecast accuracy. For example, Lopez-Restrepo et al. (2020) calibrated the spatial length scale of the covariance localization and the temporal length scale of the stochastic model for the emission uncertainty of EnKF and assimilated ground-level $PM_{2.5}$ and PM_{10} data with an optimized assimilation system to improve the simulation and forecasting of $PM_{2.5}$ and PM_{10} in a densely populated urban valley of the tropical Andes. Park et al. (2022) developed a DA system for the CTM using the EnKF technique, where $PM_{2.5}$ observations from ground stations are assimilated to ICs every 6 hours to improve $PM_{2.5}$ forecasting in the Korean region. Peng et al. (2017) used EnKF to optimize ICs and emission input, resulting in significant improvements in $PM_{2.5}$ forecast. However, EnKF also requires an appropriately sized ensemble. A small ensemble introduces significant sampling error, while an excessive ensemble consumes considerable computational resources.

For low dimensional linear dynamical systems, standard techniques are used to achieve DA, such as KF, or the adjoint methods. However, the CTMs are strongly nonlinear systems, and the assumptions of Gaussian variables and non-biased do not apply. Advanced DA techniques such as 4D-Var, EnKF are approximately 100 times more computationally expensive than the forward model when applied to nonlinear systems(Counillon and Bertino, 2009). Moreover, the Coupled chemistry meteorology models (CCMM) are CTMs that simulate meteorological processes and chemical transformations jointly, with model computations far exceeding those of equivalent weather models, and it will be a great challenge to establish a real-time and operational DA system. Compared to EnKF, EnOI is a suboptimal method for ensemble-based assimilation (Evensen, 2003). EnOI uses a stationary ensemble to estimate the BEC and only one analysis field (AF) is updated at a time, which makes the computation greatly reduced. EnOI is robust, flexible, portable, and inexpensive, and is not burdened with the technical difficulties that some other methods carry. EnOI can be used in conjunction with other DA methods and may be an appropriate choice for coupled forecast systems(Oke et al., 2010). EnOI has been widely used in ocean models with significant improvements to model forecast (Counillon and Bertino, 2016; Castruccio et al., 2020; Xie and Zhu, 2010b; Belyaev et al., 2021), but the actual operational use in CTMs is still relatively rare. In this study, we established a real-time EnOI chemistry initial fields $PM_{2.5}$ assimilation system for GRAPES_Meso5.1/CUACE to assimilate $PM_{2.5}$ data from nearly 1500 ground stations in China into the model chemical initial fields to improve the model $PM_{2.5}$ forecast accuracy and discuss the impact of assimilating $PM_{2.5}$ on visibility.

https://doi.org/10.5194/gmd-2022-207
Preprint. Discussion started: 7 November 2022


Geoscientific Model Development Discussions

2 Methods and Data

2.1 EnOI

DA methods are algorithms for optimal estimation. They combine observations and model results and their respective statistical characteristics of errors to obtain a statistically optimal analysis value by minimizing the analysis variance. Based on Kalman filter theory, the sequential assimilation methods use Eq. (1) to update the state variables.

$$\boldsymbol{x}^a = \boldsymbol{x}^b + \mathbf{K}(\mathbf{y} - \mathbf{H}(\mathbf{x}^{\mathrm{b}})) \quad (1)$$

Where the model forecast and analysis are denoted as $\boldsymbol{x}^a$ and $\boldsymbol{x}^b$, respectively, and the measurements are contained in $\mathbf{y}$. The observation operator $\mathbf{H}$ is the spline or other interpolations from the initial fields $PM_{2.5}$ to the observational space. $\mathbf{K}$ is the Kalman gain matrix. $\boldsymbol{\psi}_i = (\mathrm{i} = 1, \cdots, \mathrm{N})$ is an n-dimensional model state vector representing members of the ensemble. N ensemble samples are combined in an ensemble $\boldsymbol{A}$.

$$\boldsymbol{A} = (\boldsymbol{\psi}_1, \boldsymbol{\psi}_2, \cdots, \boldsymbol{\psi}_N) \in \mathfrak{R}^{n \times N} \quad (2)$$

$$\overline{\boldsymbol{A}} = \boldsymbol{A}\boldsymbol{E}_N \in \mathfrak{R}^{n \times N} \quad (3)$$

Where $\overline{\boldsymbol{A}}$ is the ensemble mean, and the ensemble anomaly $\boldsymbol{A}'$ is then defined as

$$\boldsymbol{A}' = \boldsymbol{A} - \overline{\boldsymbol{A}} = \boldsymbol{A}(\boldsymbol{I} - \boldsymbol{E}_N) \in \mathfrak{R}^{n \times N} \quad (4)$$

Where $\boldsymbol{E}_N$ is an N × N matrix with each element being 1/N.

EnOI is approximate to EnKF. This involves using a stationary historical ensemble to define BEC matrix $\boldsymbol{B}$.

$$\boldsymbol{B} = \frac{\boldsymbol{A}'\boldsymbol{A}'^T}{\mathrm{N}-1} \in \mathfrak{R}^{n \times n} \quad (5)$$

As in Evensen (2003), the EnOI analysis is computed by solving an equation written as:

$$\boldsymbol{\psi}^a = \boldsymbol{\psi}^f + \alpha(\boldsymbol{A}'\boldsymbol{A}'^T)\boldsymbol{H}^T[(\alpha\boldsymbol{H}(\boldsymbol{A}'\boldsymbol{A}'^T)\boldsymbol{H}^T + (\mathrm{N}-1)\boldsymbol{R})]^{-1}(\boldsymbol{d} - \boldsymbol{H}\boldsymbol{\psi}^f) \quad (6)$$

The analysis is now computed to update only one model state at a time. As in Eq. (1), $\boldsymbol{\psi}^a$ is the AF, $\boldsymbol{\psi}^f$ is background field (BF), $\boldsymbol{d}$ is the measurements. $\mathbf{R}$ is the measurement error covariance. $(\boldsymbol{d} - \boldsymbol{H}\boldsymbol{\psi}^f)$ is the forecast innovation. A scalar $\alpha \in (0, 1]$ is used to adjust the weight between the measurement and the ensemble, and α is taken as 0.9 in this study.

The ensemble-based methods use ensemble samples to approximate the BEC. Finite samples can introduce spurious information, and reasonable and effective methods are needed to remove spurious correlation information as much as possible. Also, to avoid all observations affecting the same model grid, a localization scheme is used to solve this problem. Localization can delete those long distance correlations in the BEC matrix, and limit the influence of a single observation by the Kalman update equation within a fixed region around the observation location(Xie and Zhu, 2010a). Localization also can increase the rank of the forecast error covariance and improve performance(Oke et al., 2002). In this study, for an analysis grid point, only

https://doi.org/10.5194/gmd-2022-207
Preprint. Discussion started: 7 November 2022


Geoscientific Model Development Discussions

those observations within the localization length-scale are considered, then the Kalman increments of the observations to the grid point are calculated separately. The weight coefficients based on the distance between the observation and the model grid point are calculated for assimilation at the end. The observations can be reused.

Based on the EnOI Eq. (6), we built the EnOI initial field $PM_{2.5}$ assimilation system, as shown in Fig. 1. The main procedures can be divided into pre-processing, analysis, and post-processing. Pre-processing involves the acquisition of observed data and ensemble samples. Analysis is the revised main module of EnOI where the main computational processes are performed. Post-processing processes the results obtained from assimilation into model-readable chemical ICs to preliminarily verify the assimilation results. Compared with the traditional EnOI, the time-continuous historical samples before the assimilation moment are selected as the ensemble samples for this study. The BEC is stationary for a particular analysis moment, but it changes with the assimilation moment during a long assimilation period.

2.2 GRAPES_Meso5.1/CUACE

In this study, the DA method EnOI was established for the updated version of the regional atmospheric chemistry model GRAPES_Meso5.1/CUACE developed by the China Meteorological Administration. The model has been widely used to study dust and haze prediction, aerosol radiation, and aerosol-cloud interactions (Wang et al., 2008; Wang et al., 2010a; Wang et al., 2010b; Wang and Niu, 2013; Wang et al., 2015; Zhou et al., 2012; Wang et al., 2018; Peng et al., 2020; Peng et al., 2021b; Zhai et al., 2018; Zhang et al., 2022). For the dynamic frame, the model uses a full compressible non-hydrostatic model core, an Arakawa C staggered grid, an improved material advection scheme of the Piecewise Rational function Method(Peng et al., 2005), and a height-based terrain-following coordinate. The chemical module uses the CUACE, which consists of an emission inventory system, CAM aerosols module, Regional Acid Deposition Model (RADM2) and gases-particles transformation-related processes. In the RADM2, 63 gas species through 21 photochemical reactions and 136 gas-phase reactions participate in the calculations. CAM module considers the dynamic, physical and chemical processes of aerosols including hygroscopic growth, dry and wet depositions, condensation, nucleation, etc (Gong and Zhang, 2008). Seven types of aerosols (sea salt, sand/dust, black carbon, organic carbon, sulfate, nitrate, and ammonium salt) are considered in the CAM. The aerosol size spectrum (except for ammonium salt) is divided into 12 bins with particles radium of 0.005–0.01, 0.01–0.02, 0.02–0.04, 0.04–0.08, 0.08–0.16, 0.16–0.32, 0.32–0.64, 0.64–1.28, 1.28–2.56, 2.56–5.12, 5.12–10.24, and 10.24–20.48 μm.

2.3 Data used

A severe haze episode occurs in Northern China from 15 to 23 December 2016. During this pollution episode, the highest daily $PM_{2.5}$ concentration peaks 600 μg m^{-3} in Shijiazhuang and some other cities, reaching the severely polluted level (250-500 μg m^{-3}). In this study, this regional haze episode was selected as the study period, and both model input data and observation data used in this study are within this period. Model input data include anthropogenic emission data, model meteorological initial and boundary data. The emission inventory used in this study is from the Multi-resolution Emissions

https://doi.org/10.5194/gmd-2022-207
Preprint. Discussion started: 7 November 2022


Geoscientific Model Development Discussions

Inventory for China (MEIC) in December 2016 (http://www.meicmodel.org/). The emission inventory covers power plants, industry (cement, Iron and steel, industrial boilers, petroleum industry), residential, transportation, solvent use and agriculture, in-field crop residue burning etc. National Centers for Environmental Prediction (NCEP) Final analysis (FNLs) data (https://rda.ucar.edu/datasets/ds083.3/) are used for the model's initial and 6 h meteorological lateral boundary input fields. The observations include $PM_{2.5}$ and visibility. Nearly 1500 ground-based hourly $PM_{2.5}$ (μg m^{-3}) observations from the Chinese Ministry of Environmental Protection, with the detailed location and spatial distribution of the stations shown in Fig. 1. The hourly meteorological automatic ground-based visibility data (km) were obtained from the China Meteorological Administration. The time format of these observations is processed to UTC and all the observational data are obtained after quality control and rechecked before use.

2.4 Experimental Setup

The horizontal resolution, time step, forecast length and model domain of the GRAPES_Meso5.1/CUACE model are optional. In this study, the horizontal resolution of the model is 0.1°×0.1°, the time step is 100 s, and the model domain is15-60° E, 70-145° N and (grey dashed box in Figure 2). There are 49 model layers ascending vertically from the surface to 31km in height. The model warm restart time is 0000 UTC and 1200 UTC, and the forecast length is 24 hours. The chemical initial field of the model warm restart uses the 24-hour forecast field of the day before the model, or the chemical initial field assimilated by EnOI, and the simulation results are output on an hourly basis.

Three groups of experiments were performed in this study: one set of control experiments (CR), one set of sensitivity experiments and one set of cyclic DA experiments, as shown in Table 1. CR00 is the control experiment representing the model with a daily warm restart at 0000 UTC and without DA (the initial field is the previous day's 24-hour forecast field), simulated from 9 to 23 December 2016. The localisation length-scale L and the ensemble size N are the key parameters affecting EnOI. Based on CR00, two parallel sensitivity experiments were designed to study the impact of localisation length-scale and ensemble size on the assimilation effects. The chemical initial fields, ensemble samples for the sensitivity experiments were obtained from the CR00. The first group of sensitivity experiments is fixed with ensemble size N of 48, and length-scale is selected for 20, 40, 60, 80, and 100 km to investigate the impacts of different localization length-scale choices on the optimized chemical initial field; the second group is fixed with length-scale L of 80 km, and the 24, 48, 72, 96, 120, and 144 simulations before the assimilation moment (0000 UTC) were selected as ensemble samples, respectively, and the effect of the number of ensemble samples on the assimilation effect was discussed. Considering that the missing localization could break the model dynamical balance(Oke et al., 2007), localization was performed in selecting the optimal ensemble size. To investigate the impact of the assimilation moment on the forecast fields, the optimal length-scale and ensemble size were selected based on the results of sensitivity experiments, and two sets of cyclic DA experiments, DA00 and DA12, were set up to represent the daily assimilation of the initial fields at 0000 UTC and 1200 UTC, respectively. The N hourly model forecasts before the assimilation moment were used as the ensemble samples to approximate the BEC, and the analysis increments are calculated by combining the model forecasts and $PM_{2.5}$ observations at 0000 UTC and 1200 UTC, and the revised AFs are

https://doi.org/10.5194/gmd-2022-207
Preprint. Discussion started: 7 November 2022


Geoscientific Model Development Discussions

used as the chemical initial fields for the next forecast to achieve cyclic DA. To avoid errors caused by different warm restart times, the CR12 control experiment is set up to represent a daily warm restart at 1200 UTC but without assimilation to be used as a reference experiment for DA12.

3 Result and discussion

3.1 Localisation length-scale sensitivity experiments

The aspect of localisation needs to be adapted for specific applications, so two observation sites A (114.5° E, 38.0° N), and B (36.6° N, 116.9° E) were selected to perform a length-scale single-point experiment for the initial field at 0000 UTC on 15 December 2016, corresponding to the left and right columns of the analysis increments ($\boldsymbol{\psi}^a - \boldsymbol{\psi}^f$) shown in Fig. 3. The analysis increments are determined by both the observation increments and the BEC based on Eq. (6). As shown in Fig. 3, the increments are positive in the left and negative in the right column, which represent the underestimation of $PM_{2.5}$ concentration at site A and overestimation at site B before being assimilated. As the length-scale increases, the range of analysis increment expands, and the number of model grids that can be affected increases gradually. Due to the sparse distribution of $PM_{2.5}$ sites, if the localization length-scale is too small, most of the model grids cannot be updated, which reduces the assimilation efficiency; whereas if the localisation length-scale is too large, the analysis increments between distant sites will offset and superimpose, creating fake increments. With the experiments using length-scale of L = 80 and 100 km, a small negative analysis increments are found at site A in the southeast direction. Compared to site A, a wide positive analysis increments that do not match the actual situation are found at site B in the west direction for experiments using L=60, 80, and 100km. Clearly too large a localization radius can lead to error increments. It is worth noting that there are differences in the shape of the analysis increment fields at sites A and B, which is related to the EnOI having a flow-dependent BEC, the details of BEC will be discussed in 3.2.

To obtain the statistically optimal localization length-scale, the initial fields from 15 to 23 December 2016 were performed for sensitivity experiments, respectively, and the results are shown in Fig. 4. The more the scatter points are clustered on the diagonal line means that more the simulation is closer to the observation. Compared to the CR, the scatter distribution of the DA experiments is closer to the diagonal, with Correlation Coefficient (CORR) closer to 1, and the Root Mean Square Error (RMSE), Mean Bias (MB), and Mean Error (ME) of the DA experiment are smaller than those of the CR. The statistical data are significantly different, indicating that localization can effectively improve the model forecast accuracy. When localisation is used with a 40-member ensemble and length-scale of 40km, the RMSE is 18.472 μg m^{-3}, ME is 10.481 μg m^{-3}, and CORR is 0.977, which is the best among all the experiments on different length-scale. For experiments with length-scale of 20, 40, 60, 80 and 100 km MB is 2.656, 1.973, and1.928, 2.194, 1.985 μg m^{-3}, respectively. Ground-based $PM_{2.5}$ sites are established according to the population and economic development level of the region, and are not evenly distributed, such as Beijing, Shanghai, Guangzhou, and other economically developed and populous megacities, which have a high density of $PM_{2.5}$ sites, while the western and central regions of China are sparsely populated, and the sites are partially sparse. Using a localization

https://doi.org/10.5194/gmd-2022-207
Preprint. Discussion started: 7 November 2022


Geoscientific Model Development Discussions

length-scale of 20 km prevents most of the model data from being updated while using too large a length-scale allows remote sites to interact with each other and produce spurious increments. In addition, from the meteorological conditions, heavy pollution weather is always characterized by small or static winds, pollutant transport over small distances, an observation site represents a limited spatial extent, so a larger localized length-scale setting may also produce an unreasonable initial field. In summary, we concluded that the best assimilation effect can be achieved when the localization length-scale is using 40 km.

3.2 Ensemble size sensitivity experiments

We repeat the series of experiments presented in Fig. 3, but with a localising length-scale of 80 km and 24, 48, 72, 96 and 120 ensemble members. Figure 5 shows a map of CORR between observation sites (A, B) and BECs for different ensemble size, overlaid with the 0000 UTC surface wind vector of 15 December 2016. Site A is controlled by strong north and northwest winds, which makes the r field show a northeast-southwest trend; The wind speed at site B is less than 5 $m.s^{-1}$ in all directions with a steady state, so the CORR field is approximately distributed in concentric circles nearby the center of the site. As the number of ensemble samples increases, the range of positive CORR at sites A and B gradually increases with the range of CORR greater than 0.7. The ensembles of size N =24 or N=48 can be considered small, in this case, the CORRs between the observation sites and the surrounding large-scale areas are all greater than 0.7, and an extremely strong negative correlation is found in the southwest, which exaggerates the correlation of each area. The success of ensemble-based DA systems depends strongly on the number of samples. The smaller ensemble size fails to accurately estimate the BEC and is prone to sampling error, resulting in unreasonable results, and Natvik and Evensen (2003) investigated the effect of the number of samples on assimilation and showed that an ensemble of fewer than 60 samples reduce the performance of assimilation. When the hourly model forecasts of over 5 days (N=120) before assimilation are selected as the ensemble samples, the correlations of both sites A and B with the BECs in a wide area become positive.

Next, all $PM_{2.5}$ sites were used to assimilate the initial field at 0000 UTC per day for this pollution episode, and six different ensemble sizes were used to improve the initial field as shown in Table 2. Compared with the unassimilated initial field, the RMSE, CORR, MB, and ME of the initial field after assimilation changed significantly. With only 24 ensemble samples assimilated, the RMSE rapidly decreased from 71.776 to 20.675 μg m^{-3}, and the CORR directly increased from 0.650 to 0.97, meanwhile the ME and MB were 1⁄4 and 1⁄9 of the original. When 120 samples were selected for assimilation, the analysis field $PM_{2.5}$ statistics were worse than those of fewer samples (N=24, 48, 72, 96, 144). The RMSEs for 24, 120, and 144 samples were 20.675, 23.919, and 23.416 μg m^{-3} respectively, and the CORRs were also less than 0.96, and the RMSE results for 48, 72, and 96 ensemble samples are 19.170, 18.908, and 18.849 μg m^{-3} respectively. The differences between the statistics also indicate there is an optimal ensemble size, the RMSE of the experiment using 96 samples is smaller than the RMSE when using the other ensemble sizes, and the remaining statistics are better than the results when other samples are selected, so we consider that the best assimilation is achieved when the number of ensemble size is 96.

https://doi.org/10.5194/gmd-2022-207
Preprint. Discussion started: 7 November 2022


Geoscientific Model Development Discussions

3.3 Impact on initial fields

The optimal localization length-scale, ensemble size of 40 km and 96 were obtained by sensitivity experiments, respectively. In order to verify the assimilation effect, firstly, an independence test with length-scale of L=40 and ensemble size of N= 96 was performed on the initial field of 0000 UTC on 15 December 2016. The 50% of $PM_{2.5}$ sites were randomly selected as DA sites, and the rest were used as verification sites (without DA), and the blue and red sites shown in Figure 2 represent the spatial distribution of verification and assimilation sites, respectively. As shown in Figure 6, the CORRs of the verification sites and DA sites before assimilation were 0.441 and 0.470, respectively, and the RMSEs were 59.914 μg m^{-3} and 62.783 μg m^{-3}, respectively. After the DA sites were assimilated, the CORR of assimilated sites increased to 0.977 and the RMSE decreased to 14.140 μg m^{-3}, also the CORR of verification sites increased to 0.734 and the RMSE decreased to 46.041 μg m^{-3}. It is obvious that the assimilation corrected the initial $PM_{2.5}$ concentration significantly, especially in the region underestimate, and assimilating not only produces mainly localized increment structures concentrated around the measurement sites, but also affects other areas.

As in sensitivity experiments, all $PM_{2.5}$ sites were used as DA sites to assimilate the initial fields in the CR00 experiment separately, but with a localization length-scale of 40 km and an ensemble size of 96. To understand the assimilation effect of different pollution levels, we consider this episode from 15 to 23 December 2016, the first two days as the pollution start period, days 3 to 7 as the pollution period, and the last two days as the pollution dissipation period. In this section, we show in Fig. 7 the spatial distribution of $PM_{2.5}$ in the observation field (OB), BF, AF, and AFI for two days of light pollution (Dec. 16, 23) and two days of heavy pollution (Dec. 19, 20). The black boxed area in Fig.7 is the same as North China (NC) in Fig. 2, including Beijing, Tianjin, eastern Shanxi, southern Hebei, western Shandong, and northern Henan, which has the highest simulated $PM_{2.5}$ concentration. Compared with OBs, the BFs $PM_{2.5}$ is generally overestimated in NC and eastern China during the pollution start and dissipation periods. During the heavy pollution period, the BFs $PM_{2.5}$ concentrations are overestimated in northeast China and underestimated in NC. After assimilating the BFs, the AFs $PM_{2.5}$ concentration distribution changes from sheet-like to discrete, which is due to the update of the model data in a length-scale of 40 km range with the distribution of observation sites, resulting in the adjustment of the $PM_{2.5}$ in the BFs. Negative values of the AFI demonstrate that assimilation reduces $PM_{2.5}$ concentrations, while positive values demonstrate that assimilation increases $PM_{2.5}$ concentrations. During the period before and after pollution, $PM_{2.5}$ concentrations decrease in eastern China and increase in western China and NC, indicating that the reduction of the overestimation or underestimation of the model simulation over these regions with data assimilation.

To evaluate quantitatively the impact of the ensemble assimilation system on the initial fields, the RMSEs, MEs, MBs and CORRs of the assimilated initial fields and the BFs were first analysed. Table 3 shows the statistics for the two regions of the initial field, the China mainland (Total) and NC (Contains observation sites in NC). In China mainland, ME, and RMSE decreased by 75.53%, 72.33%, respectively, and CORR increased to 0.967. The MB changes from negative to positive, meanwhile the MB in mainland China becomes larger. In NC, MB decreased by 109.63%, ME decreased by 79.59%, RMSE

https://doi.org/10.5194/gmd-2022-207
Preprint. Discussion started: 7 November 2022


Geoscientific Model Development Discussions

decreased to about 20 μg m^{-3}, and CORR increased by 148.59%. The results show that the correction effect of DA on the initial fields is evident.

3.4 Impact on forecast fields

3.4.1 Impact on $PM_{2.5}$ forecast fields

In this section, we will investigate the performance of assimilating the initial field at 0000 UTC per day (DA00) or 1200 UTC per day (DA12) on improving the $PM_{2.5}$ forecasts, with an example in North China (Figure 8), and the same study period as in section 3.3 was selected, DA00 (Figure 8 First and second rows) and DA12 (Figure 8 third and fourth rows) were performed in parallel. In NC, compared with the observations (brown line with circles), the forecast $PM_{2.5}$ concentrations (black line, grey line) are 20 to 100 μg m^{-3} higher in the pollution start period (16 December) and the pollution fading period (23 December), lower in the pollution period (19 December), and relatively consistent in (20). The daily trend of $PM_{2.5}$ changes immediately one hour after 0000UTC in DA00 (blue line) or 1200UTC in DA12 (pink line), and the assimilation forecast value rapidly approaches the observations, after that the DA experiment gradually overlaps with the CR experiments in the context of daily changes of emission. It can be seen from Fig. 8 that the RMSEs of the DA experiments (blue and pink lines marked with squares) are always lower than that of the CR experiments (black and grey lines marked with squares), which proves that assimilating the initial field improves the $PM_{2.5}$ forecast field throughout the assimilation time window, yet the assimilation impact is strongest in the first 12 hours. The comparison reveals that the assimilation effect is related to the choice of the assimilation moment, and the blank area between the RMSE line of the DA experiment and the RMSE line of the CR experiment represents the improvement of the DA on the forecast, and the larger the blank area is, the greater the improvement of the DA on the forecast. For example, the model forecast at 0000UTC on 19 December is closer to the observation, and assimilating the initial field at 0000UTC does not improve the model forecast significantly; instead, the model is about 100 μg m^{-3} lower than the observation at 1200UTC, and the model's forecast improves more after assimilating the initial field at 1200UTC.

The daily average of the 24-hour RMSE was obtained for the DA and CR experiments, the relative RMSE was calculated and plotted in a daily time series histogram as shown in Fig. 9. The red and blue bars represent the percentage improvement of the original forecasts after assimilation, and the white diagonal bars represent the difference between the improvements of DA00 and DA12. In this episode, the improvement of China mainland $PM_{2.5}$ forecasts by DA00 and DA12 are minimum at 9% and 10% respectively on December 15 and maximum at 15% and 21% respectively on December 19. The minimum and maximum improvement of assimilation on $PM_{2.5}$ forecasts in NC both appear in DA12, which are 3% and 25%, respectively. The difference between DA12 and DA00 relative RMSEs is mostly positive, within 6% in China mainland, but in NC this difference can be up to 15%. The study shows that assimilating the initial field at 1200 UTC improves the $PM_{2.5}$ forecast more than 0000 UTC, mainly because the model forecasts are not close to the observations at 1200 UTC in most cases (Figure 8), thus choosing this time for assimilation will have a significant impact. The selection of the assimilation moment can be disregarded in the

https://doi.org/10.5194/gmd-2022-207
Preprint. Discussion started: 7 November 2022


Geoscientific Model Development Discussions

case of abundant computing resources because, with the increase of assimilation frequency, it can also achieve good results, but in the case of limited computing resources, choosing the suitable assimilation moment can save computing resources as well as improve the forecast accuracy.

3.4.2 Impact on Visibility forecast fields

The occurrence of low visibility episodes is usually associated with aerosol pollution. The horizontal spatial distribution of the OBs, forecast fields without assimilation (CR), forecast fields with assimilation (DA), and incremental fields (DA-CR) for visibility and $PM_{2.5}$ at 0100 UTC on 16 and 20 December are shown in Fig.10. During the pollution start period (16 December 0100 UTC) visibility is above 10km in most of China, and during the pollution period (20 December 0100 UTC) visibility is mostly below 7km in eastern China. After assimilating the ground-based $PM_{2.5}$, the visibility distribution of DAs becomes discrete compared to the CRs. A positive $PM_{2.5}$ concentration increment corresponds to a negative visibility increment, that means that when the $PM_{2.5}$ concentration increases, the visibility decreases at the same moment. At 0100UTC On 16 December, the CR $PM_{2.5}$ concentration is underestimated in NC and overestimated in Southeast China, and after assimilating $PM_{2.5}$, the visibility is reduced in NC with increased $PM_{2.5}$ and increased in Southeast with reduced $PM_{2.5}$. In the period of light pollution, the absolute value of visibility increment is mostly in the range of 5-7 km when the $PM_{2.5}$ increment is from 30 to 110 μg m^{-3} or from -30 to -110 μg m^{-3} in NC, while in the pollution period (20 December 0100 UTC for example), under the same $PM_{2.5}$ analysis increment, the visibility increment in NC is between -3 and 3 km. It proves that visibility is more correlated with $PM_{2.5}$ concentration when the pollution is lighter, while they are less correlated when the pollution is heavier, which is consistent with the findings of Yu et al. (2016)and Yadav et al. (2022).

Four stations, Beijing (BJ), Shijiazhuang (SJZ), Xingtai (XT), and Jinan (JN), were selected from the heavily polluted NC to study the effect of assimilating the initial field $PM_{2.5}$ on the visibility forecasts. Since the assimilation effect is most obvious in the first 12 hours, we focus on the improvement of visibility forecasts within 12 hours. Figure 11 shows the observation (orange line), simulation (black dashed line) and assimilation (green line) of visibility and observation (grey line), simulation (black line) and assimilation (blue line) of $PM_{2.5}$ concentration for the above cities from 0100 to 1200 on 16 and 20 December 2016. On 16 December, when $PM_{2.5}$ concentration is less than 300 μg m^{-3} (December 16), visibility at all four stations is closer to the observed value by assimilating $PM_{2.5}$, among which BJ and JN have decreased $PM_{2.5}$ concentration after assimilation, and visibility has increased at the same time. SJZ and XT have increased $PM_{2.5}$ concentration and decreased visibility after assimilation. In the period of low $PM_{2.5}$ concentration, about 100 μg m^{-3} $PM_{2.5}$ change makes visibility change 11km, 4km, 5km and 7km in BJ, SJZ, XT and JN respectively. In the period of heavy pollution, $PM_{2.5}$ concentration change 150 μg m^{-3} in Beijing and Shijiazhuang at 0100UTC, while visibility change 3.5km and 0.5km respectively. It is obvious that the improvement of visibility by assimilating $PM_{2.5}$ is limited during the heavy pollution period. It is worth noting that when the $PM_{2.5}$ concentration is greater than 350 μg m^{-3} at the JN site, although the decrease of $PM_{2.5}$ concentration corresponds to the increase in visibility, the gap between the assimilated visibility and observation becomes larger at this time, which may be related to the inaccuracy of the humidity simulation here and inaccurate visibility parameterization scheme for the model.

https://doi.org/10.5194/gmd-2022-207
Preprint. Discussion started: 7 November 2022


Geoscientific Model Development Discussions

Visibility is not linearly related to $PM_{2.5}$, and visibility is also affected by humidity and other factors. Assimilation of the initial field $PM_{2.5}$ can improve the visibility forecast, but if we want to improve the visibility forecast significantly, other objects of assimilation, such as PM_{10}, humidity, etc., need to be considered.

4 Conclusions

To improve the accuracy of $PM_{2.5}$ and visibility forecasting in China, a real-time and efficient EnOI assimilation system is established for the latest online operational chemistry weather model GRAPES_Meso5.1/CUACE of China Meteorological Administration. The ground-based $PM_{2.5}$ observation data nearly 1500 surface stations covering the whole country are used for assimilation. $PM_{2.5}$ and visibility simulation-assimilation experiments were performed for a haze pollution episode from 15 to 23 December 2016. Parallel sensitivity experiments of localization length-scale and ensemble size were set up to determine two key parameters that influence the effectiveness of EnOI assimilation. Based on the results of sensitivity experiments, the initial fields were assimilated at 0000 UTC each day from 15 to 23 December 2016 to study the improvement of EnOI on the initial field $PM_{2.5}$. In addition to the analysis of the China mainland assimilation effect, the heavily polluted North China was additionally divided to discuss the different impacts of assimilation on the overall and regional chemical initial fields. Cyclic assimilation experiments were performed at 0000 UTC (DA00) and 1200UTC(DA12) to investigate the impacts of assimilation on the forecast fields, taking NC as an example, to discuss the impacts of assimilation on $PM_{2.5}$ and visibility forecast fields.

The optimal localization length-scale and the number of ensemble samples are 40 km and 96, respectively, derived from sensitivity experiments. The DA can significantly improve the model initial field, the AFs $PM_{2.5}$ is more consistent with the observed results in both distribution and values. The AFs relative to the background fields (BFs) in China mainland, NC the ME decreased by almost 80%, the RMSE decreased by 72.33%, 75.53%, the CORR increased from 0.584 to 0.967, and 0.319 increased to 0.972. The results of the DA00, DA12 assimilation experiments showed that the improved impacts of the DA worked throughout the forecast time window, but the assimilation impact was most pronounced in the first 12 hours and gradually decreased in the subsequent time. Within the 24-hour forecast time window, the average RMSE improvement for the China mainland $PM_{2.5}$ forecast field ranges from 9% to 21%, and between 4% and 25% in NC, and the comprehensive comparison shows that the initial field of 1200 UTC assimilation is superior to 0000 UTC. Therefore, in this study, it is considered that with limited computational resources, the ENOI assimilation efficiency is highest with the largest distance between the model simulation and observation to assimilate according to the model characteristics. When it comes to operational use, the assimilation efficiency can be improved by shortening the assimilation time interval due to the small demand of EnOI computational resources.

The assimilation of $PM_{2.5}$ has a significant improvement on visibility forecasts, with different degrees of visibility improvement in different cities. When the $PM_{2.5}$ increment by assimilation is negative, it corresponds to an increase in visibility, and when the $PM_{2.5}$ analysis increment is positive, visibility decreases correspondingly. The greater the change in $PM_{2.5}$ concentration

https://doi.org/10.5194/gmd-2022-207
Preprint. Discussion started: 7 November 2022


Geoscientific Model Development Discussions

during periods of light pollution, the more pronounced the improvement in visibility, but this positive correlation is not particularly obvious during periods of heavy pollution. However, it is worth noting that visibility is related to a variety of factors. Assimilating only ground-based $PM_{2.5}$ sites has a limited effect on visibility, and we will further consider assimilating PM_{10}, humidity and other meteorology factors to improve visibility forecasts in subsequent studies. In addition, the number of ground-based $PM_{2.5}$ sites is not large enough in most region of China, and we will consider assimilating $PM_{2.5}$ and satellite AOD data simultaneously at a later stage to achieve more accurate $PM_{2.5}$ and visibility forecasts.

Code and data availability. The EnOI method and related processes written in Fortran language and observation data used in this research are available at https://doi.org/10.5281/zenodo.7002847. The National Centers for Environmental Prediction Global Final Analysis (NCEP-FNL) data are available online (https://rda.ucar.edu/datasets/ds083.2/ and https://rda.ucar.edu/datasets/ds083.3/). The emission inventories are available online (http://www.meicmodel.org/).

Author contributions. LST: Validation, Formal analysis, Writing - Original Draft, Visualization, Investigation, Software. WP: Conceptualization, Methodology, Software, Writing - Original Draft. WH: Conceptualization, Methodology, Supervision, Writing- Reviewing and Editing. PY: Validation, Software. LZD and ZWJ: Validation. LHL: Data Curation. WYQ and CCHZ: Resources. ZXY: Supervision

Competing interests. The contact author has declared that neither they nor their co-authors have any competing interests.

Acknowledgements. This study is supported by the National Key Research and Development Program （2019YFC0214603, 2019YFC0214601) and the NSFC for distinguished young scholars (41825011). We also appreciate the comments of the reviewers that helped us to improve this article.

References

Belyaev, K., Kuleshov, A., Smirnov, I., and Tanajura, C. A. S.: Generalized Kalman Filter and Ensemble Optimal Interpolation, Their Comparison and Application to the Hybrid Coordinate Ocean Model, Mathematics, 9, 2371, 2021.

Bergthórsson, P. and Döös, B. R.: Numerical Weather Map Analysis1, Tellus, 7, 329-340, https://doi.org/10.1111/j.2153-3490.1955.tb01170.x, 1955.

Cao, H., Henze, D. K., Zhu, L., Shephard, M. W., Cady-Pereira, K., Dammers, E., Sitwell, M., Heath, N., Lonsdale, C., Bash, J. O., Miyazaki, K., Flechard, C., Fauvel, Y., Kruit, R. W., Feigenspan, S., Brümmer, C., Schrader, F., Twigg, M. M., Leeson, S., Tang, Y. S., Stephens, A. C. M., Braban, C., Vincent, K., Meier, M., Seitler, E., Geels, C., Ellermann, T., Sanocka, A., and Capps, S. L.: 4D-Var Inversion of European NH3 Emissions Using CrIS NH3 Measurements and GEOS-Chem Adjoint With Bi-Directional and Uni-Directional Flux Schemes, Journal of Geophysical Research: Atmospheres, 127, e2021JD035687, https://doi.org/10.1029/2021JD035687, 2022.

Carnevale, C., De Angelis, E., Finzi, G., Turrini, E., and Volta, M.: Optimal Interpolation Based Data Fusion Techniques to Improve Deterministic Air Quality Forecast, Air Pollution Modeling and its Application XXVII, Berlin, Heidelberg, 2021//, 145-150,

Castruccio, F. S., Karspeck, A. R., Danabasoglu, G., Hendricks, J., Hoar, T., Collins, N., and Anderson, J. L.: An EnOI-Based Data Assimilation System With DART for a High-Resolution Version of the CESM2 Ocean Component, Journal of Advances in Modeling Earth Systems, 12, 10.1029/2020ms002176, 2020.

Chen, D., Liu, Z., Fast, J., and Ban, J.: Simulations of sulfate–nitrate–ammonium (SNA) aerosols during the extreme

haze events over northern China in October 2014, Atmospheric Chemistry and Physics, 16, 10707-10724, 10.5194/acp-16-10707-2016, 2016.

Cheng, Y., Dai, T., Goto, D., Schutgens, N. A. J., Shi, G., and Nakajima, T.: Investigating the assimilation of CALIPSO global aerosol vertical observations using a four-dimensional ensemble Kalman filter, Atmospheric Chemistry and Physics, 19, 13445-13467, 10.5194/acp-19-13445-2019, 2019.

Counillon, F. and Bertino, L.: Ensemble Optimal Interpolation: multivariate properties in the Gulf of Mexico, Tellus A: Dynamic Meteorology and Oceanography, 61, 296-308, 10.1111/j.1600-0870.2008.00383.x, 2009.

Counillon, F. and Bertino, L.: Ensemble Optimal Interpolation: multivariate properties in the Gulf of Mexico, Tellus A: Dynamic Meteorology and Oceanography, 61, 296-308, 10.1111/j.1600-0870.2008.00383.x, 2016.

Dai, T., Cheng, Y., Suzuki, K., Goto, D., Kikuchi, M., Schutgens, N. A. J., Yoshida, M., Zhang, P., Husi, L., Shi, G., and Nakajima, T.: Hourly Aerosol Assimilation of Himawari-8 AOT Using the Four-Dimensional Local Ensemble Transform Kalman Filter, Journal of Advances in Modeling Earth Systems, 11, 680-711, 10.1029/2018ms001475, 2019.

Derber, J. C.: A Variational Continuous Assimilation Technique, Monthly Weather Review, 117, 2437-2446, 10.1175/1520-0493(1989)117<2437:Avcat>2.0.Co;2, 1989.

Evensen, G.: Sequential data assimilation with a nonlinear quasi-geostrophic model using Monte Carlo methods to forecast error statistics, Journal of Geophysical Research: Oceans, 99, 10143-10162, https://doi.org/10.1029/94JC00572, 1994.

Evensen, G.: The Ensemble Kalman Filter: theoretical formulation and practical implementation, Ocean Dynamics, 53, 343-367, 10.1007/s10236-003-0036-9, 2003.

Feng, S., Jiang, F., Jiang, Z., Wang, H., Cai, Z., and Zhang, L.: Impact of 3DVAR assimilation of surface PM2.5 observations on PM2.5 forecasts over China during wintertime, Atmospheric Environment, 187, 34-49, 10.1016/j.atmosenv.2018.05.049, 2018.

Fu, W. and Zhu, J.: Effects of Sea Level Data Assimilation by Ensemble Optimal Interpolation and 3D Variational Data Assimilation on the Simulation of Variability in a Tropical Pacific Model, Journal of Atmospheric and Oceanic Technology, 28, 1624-1640, 10.1175/jtech-d-11-00044.1, 2011.

Gandin, L. S.: Objective Analysis of Meteorological Fields, 1963.

Ghorani-Azam, A., Riahi-Zanjani, B., and Balali-Mood, M.: Effects of air pollution on human health and practical measures for prevention in Iran, J Res Med Sci, 21, 65, 10.4103/1735-1995.189646, 2016.

Gilchrist, B. and Cressman, G. P.: An Experiment in Objective Analysis, Tellus, 6, 309-318, 10.3402/tellusa.v6i4.8762, 1954.

Gong, S. L. and Zhang, X. Y.: CUACE/Dust – an integrated system of observation and modeling systems for operational dust forecasting in Asia, Atmos. Chem. Phys., 8, 2333-2340, 10.5194/acp-8-2333-2008, 2008.

Hu, X., Waller, L. A., Al-Hamdan, M. Z., Crosson, W. L., Estes, M. G., Jr., Estes, S. M., Quattrochi, D. A., Sarnat, J. A., and Liu, Y.: Estimating ground-level PM(2.5) concentrations in the southeastern U.S. using geographically weighted regression, Environ Res, 121, 1-10, 10.1016/j.envres.2012.11.003, 2013.

Kalman, R. E.: A New Approach to Linear Filtering and Prediction Problems, Journal of Basic Engineering, 82, 35-45, 10.1115/1.3662552, 1960.

Lee, L. A., Reddington, C. L., and Carslaw, K. S.: On the relationship between aerosol model uncertainty and radiative forcing uncertainty, Proc Natl Acad Sci U S A, 113, 5820-5827, 10.1073/pnas.1507050113, 2016.

Li, Z., Zang, Z., Li, Q. B., Chao, Y., Chen, D., Ye, Z., Liu, Y., and Liou, K. N.: A three-dimensional variational data assimilation system for multiple aerosol species with WRF/Chem and an application to PM_{2.5} prediction, Atmospheric Chemistry and Physics, 13, 4265-4278, 10.5194/acp-13-4265-2013, 2013.

Lin, C., Wang, Z., and J, Z.: A data assimilation method of the Ensemble Kalman Filter for use in severe dust storm forecasts over China, Atmospheric Chemistry and Physics Discussions, 7, 10.5194/acpd-7-17511-2007, 2007.

Liu, C., Zhang, S., Gao, Y., Wang, Y., Sheng, L., Gao, H., and Fung, J. C. H.: Optimal estimation of initial concentrations and emission sources with 4D-Var for air pollution prediction in a 2D transport model, Sci Total Environ, 773, 145580, 10.1016/j.scitotenv.2021.145580, 2021.

Liu, F., Tan, Q., Jiang, X., Yang, F., and Jiang, W.: Effects of relative humidity and PM2.5 chemical compositions on visibility impairment in Chengdu, China, Journal of Environmental Sciences, 86, 15-23, https://doi.org/10.1016/j.jes.2019.05.004, 2019.

Liu, Z., Liu, Q., Lin, H.-C., Schwartz, C. S., Lee, Y.-H., and Wang, T.: Three-dimensional variational assimilation of MODIS aerosol optical depth: Implementation and application to a dust storm over East Asia, Journal of Geophysical Research: Atmospheres, 116, https://doi.org/10.1029/2011JD016159, 2011.

Lopez-Restrepo, S., Yarce, A., Pinel, N., Quintero, O. L., Segers, A., and Heemink, A. W.: Forecasting PM10 and PM2.5 in the Aburrá Valley (Medellín, Colombia) via EnKF based data assimilation, Atmospheric Environment, 232, 10.1016/j.atmosenv.2020.117507, 2020.

Mauricio Agudelo, O., Viaene, P., and De Moor, B.: Improving the PM10 estimates of the air quality model AURORA by using Optimal Interpolation**This work was supported by: • Research Council KUL: CoE PFV/10/002 (OPTEC), PhD/Postdoc grants • Flemish Government: iMinds Medical Information Technologies SBO 2015 • Belgian Federal Science Policy Office: IUAP P7/19 (DYSCO, Dynamical systems, control and optimization, 2012-2017), IFAC-PapersOnLine, 48, 1154-1159, https://doi.org/10.1016/j.ifacol.2015.12.287, 2015.

https://doi.org/10.5194/gmd-2022-207
Preprint. Discussion started: 7 November 2022

Natvik, L. J. and Evensen, G.: Assimilation of ocean colour data into a biochemical model of the North Atlantic: Part 1. Data assimilation experiments, Journal of Marine Systems, 40-41, 127-153, https://doi.org/10.1016/S0924-7963(03)00016-2, 2003.

Navon, I. M.: Data Assimilation for Numerical Weather Prediction: A Review, in: Data Assimilation for Atmospheric, Oceanic and Hydrologic Applications, edited by: Park, S. K., and Xu, L., Springer Berlin Heidelberg, Berlin, Heidelberg, 21-65, 10.1007/978-3-540-71056-1_2, 2009.

Oke, P., Brassington, G., Griffin, D., and Schiller, A.: Ocean Data Assimilation: a case for ensemble optimal interpolation, Australian Meteorological and Oceanographic Journal, 59, 10.22499/2.5901.008, 2010.

Oke, P. R., Sakov, P., and Corney, S. P.: Impacts of localisation in the EnKF and EnOI: experiments with a small model, Ocean Dynamics, 57, 32-45, 10.1007/s10236-006-0088-8, 2007.

Oke, P. R., Allen, J. S., Miller, R. N., Egbert, G. D., and Kosro, P. M.: Assimilation of surface velocity data into a primitive equation coastal ocean model, Journal of Geophysical Research: Oceans, 107, 5-1-5-25, https://doi.org/10.1029/2000JC000511, 2002.

Pagowski, M. and Grell, G. A.: Experiments with the assimilation of fine aerosols using an ensemble Kalman filter, Journal of Geophysical Research: Atmospheres, 117, https://doi.org/10.1029/2012JD018333, 2012.

Panofsky, R. A.: OBJECTIVE WEATHER-MAP ANALYSIS, Journal of Atmospheric Sciences, 6, 386-392, 10.1175/1520-0469(1949)006<0386:Owma>2.0.Co;2, 1949.

Park, S. Y., Dash, U. K., Yu, J., Yumimoto, K., Uno, I., and Song, C. H.: Implementation of an ensemble Kalman filter in the Community Multiscale Air Quality model (CMAQ model v5.1) for data assimilation of ground-level PM2.5, Geosci. Model Dev., 15, 2773-2790, 10.5194/gmd-15-2773-2022, 2022.

Peng, X., Xiao, F., Ohfuchi, W., and Fuchigami, H.: Conservative Semi-Lagrangian Transport on a Sphere and the Impact on Vapor Advection in an Atmospheric General Circulation Model, Monthly Weather Review, 133, 504-520, 10.1175/mwr-2869.1, 2005.

Peng, Y., Wang, H., Hou, M., Jiang, T., Zhang, M., Zhao, T., and Che, H.: Improved method of visibility parameterization focusing on high humidity and aerosol concentrations during fog–haze events: Application in the GRAPES_CAUCE model in Jing-Jin-Ji, China, Atmospheric Environment, 222, 117139, https://doi.org/10.1016/j.atmosenv.2019.117139, 2020.

Peng, Y., Wang, H., Zhang, X., Zhao, T., Jiang, T., Che, H., Zhang, X., Zhang, W., and Liu, Z.: Impacts of PBL schemes on PM2.5 simulation and their responses to aerosol-radiation feedback in GRAPES_CUACE model during severe haze episodes in Jing-Jin-Ji, China, Atmospheric Research, 248, 10.1016/j.atmosres.2020.105268, 2021a.

Peng, Y., Wang, H., Zhang, X., Zhao, T., Jiang, T., Che, H., Zhang, X., Zhang, W., and Liu, Z.: Impacts of PBL schemes on PM2.5 simulation and their responses to aerosol-radiation feedback in GRAPES_CUACE model during severe haze episodes in Jing-Jin-Ji, China, Atmospheric Research, 248, 105268, https://doi.org/10.1016/j.atmosres.2020.105268, 2021b.

Peng, Z., Liu, Z., Chen, D., and Ban, J.: Improving PM2. 5 forecast over China by the joint adjustment of initial conditions and source emissions with an ensemble Kalman filter, Atmos. Chem. Phys., 17, 4837-4855, 10.5194/acp-17-4837-2017, 2017.

Perez, P., Menares, C., and Ramírez, C.: PM2.5 forecasting in Coyhaique, the most polluted city in the Americas, Urban Climate, 32, 10.1016/j.uclim.2020.100608, 2020.

Piovani, C.: The "Greening" of China: Progress, Limitations, and Contradictions, Journal of Contemporary Asia, 47, 93-115, 10.1080/00472336.2016.1203011, 2017.

Sahu, S. K. and Kota, S. H.: Significance of PM2.5 Air Quality at the Indian Capital, Aerosol and Air Quality Research, 17, 588-597, 10.4209/aaqr.2016.06.0262, 2017.

Skachko, S., Ménard, R., Errera, Q., Christophe, Y., and Chabrillat, S.: EnKF and 4D-Var data assimilation with chemical transport model BASCOE (version 05.06), Geoscientific Model Development, 9, 2893-2908, 10.5194/gmd-9-2893-2016, 2016.

Talagrand, O. and Courtier, P.: Variational Assimilation of Meteorological Observations With the Adjoint Vorticity Equation. I: Theory, Quarterly Journal of the Royal Meteorological Society, 113, 1311-1328, https://doi.org/10.1002/qj.49711347812, 1987.

Tang, X., Zhu, J., Wang, Z. F., and Gbaguidi, A.: Improvement of ozone forecast over Beijing based on ensemble Kalman filter with simultaneous adjustment of initial conditions and emissions, Atmos. Chem. Phys., 11, 12901-12916, 10.5194/acp-11-12901-2011, 2011.

Tang, X., Zhu, J., Wang, Z., Gbaguidi, A., Lin, C., Xin, J., Song, T., and Hu, B.: Limitations of ozone data assimilation with adjustment of NOx emissions: mixed effects on NO2 forecasts over Beijing and surrounding areas, Atmos. Chem. Phys., 16, 6395-6405, 10.5194/acp-16-6395-2016, 2016.

Tang, Y., Chai, T., Pan, L., Lee, P., Tong, D., Kim, H.-C., and Chen, W.: Using optimal interpolation to assimilate surface measurements and satellite AOD for ozone and PM2.5: A case study for July 2011, Journal of the Air & Waste Management Association, 65, 1206-1216, 10.1080/10962247.2015.1062439, 2015.

Ting, Y.-C., Young, L.-H., Lin, T.-H., Tsay, S.-C., Chang, K.-E., and Hsiao, T.-C.: Quantifying the impacts of PM2.5 constituents and relative humidity on visibility impairment in a suburban area of eastern Asia using long-term in-situ measurements, Science of The Total Environment, 818, 151759, https://doi.org/10.1016/j.scitotenv.2021.151759, 2022.

Tombette, M., Mallet, V., and Sportisse, B.: PM₁₀ data assimilation over Europe with the optimal interpolation method, Atmos. Chem. Phys., 9, 57-70, 10.5194/acp-9-57-2009, 2009.

Wang, C., An, X., Hou, Q., Sun, Z., Li, Y., and Li, J.: Development of four-dimensional variational assimilation system based on the GRAPES–CUACE adjoint model (GRAPES–CUACE-4D-Var V1.0) and its application in emission inversion, Geosci. Model Dev., 14, 337-350, 10.5194/gmd-14-337-2021, 2021.

Wang, D., You, W., Zang, Z., Pan, X., He, H., and Liang, Y.: A three-dimensional variational data assimilation system for a size-resolved aerosol model: Implementation and application for particulate matter and gaseous pollutant forecasts across China, Science China Earth Sciences, 63, 1366-1380, 10.1007/s11430-019-9601-4, 2020.

Wang, H. and Niu, T.: Sensitivity studies of aerosol data assimilation and direct radiative feedbacks in modeling dust aerosols, Atmospheric Environment, 64, 208-218, 10.1016/j.atmosenv.2012.09.066, 2013.

Wang, H., Zhang, X., Gong, S., Chen, Y., Shi, G., and Li, W.: Radiative feedback of dust aerosols on the East Asian dust storms, Journal of Geophysical Research: Atmospheres, 115, https://doi.org/10.1029/2009JD013430, 2010a.

Wang, H., Peng, Y., Zhang, X., Liu, H., Zhang, M., Che, H., Cheng, Y., and Zheng, Y.: Contributions to the explosive growth of PM2.5 mass due to aerosol–radiation feedback and decrease in turbulent diffusion during a red alert heavy haze in Beijing–Tianjin–Hebei, China, Atmos. Chem. Phys., 18, 17717-17733, 10.5194/acp-18-17717-2018, 2018.

Wang, H., Xue, M., Zhang, X. Y., Liu, H. L., Zhou, C. H., Tan, S. C., Che, H. Z., Chen, B., and Li, T.: Mesoscale modeling study of the interactions between aerosols and PBL meteorology during a haze episode in Jing-Jin-Ji (China) and its nearby surrounding region - Part 1: Aerosol distributions and meteorological features, Atmospheric Chemistry & Physics, 15, 3257, 10.5194/acp-15-3257-2015, 2015.

Wang, H., Gong, S., Zhang, H., Chen, Y., Shen, X., Chen, D., Xue, J., Shen, Y., Wu, X., and Jin, Z.: A new-generation sand and dust storm forecasting system GRAPES_CUACE/Dust: Model development, verification and numerical simulation, Chinese Science Bulletin, 55, 635-649, 10.1007/s11434-009-0481-z, 2010b.

Wang, P., Wang, H., Wang, Y. Q., Zhang, X. Y., Gong, S. L., Xue, M., Zhou, C. H., Liu, H. L., An, X. Q., Niu, T., and Cheng, Y. L.: Inverse modeling of black carbon emissions over China using ensemble data assimilation, Atmospheric Chemistry and Physics, 16, 989-1002, 10.5194/acp-16-989-2016, 2016.

Wang, Y. Q., Zhang, X. Y., Gong, S. L., Zhou, C. H., Hu, X. Q., Liu, H. L., Niu, T., and Yang, Y. Q.: Surface observation of sand and dust storm in East Asia and its application in CUACE/Dust, Atmos. Chem. Phys., 8, 545-553, 10.5194/acp-8-545-2008, 2008.

Xiao, Q., Geng, G., Liang, F., Wang, X., Lv, Z., Lei, Y., Huang, X., Zhang, Q., Liu, Y., and He, K.: Changes in spatial patterns of PM2.5 pollution in China 2000-2018: Impact of clean air policies, Environ Int, 141, 105776, 10.1016/j.envint.2020.105776, 2020.

Xie, J. and Zhu, J.: Ensemble optimal interpolation schemes for assimilating Argo profiles into a hybrid coordinate ocean model, Ocean Modelling, 33, 283-298, https://doi.org/10.1016/j.ocemod.2010.03.002, 2010a.

Xie, J. and Zhu, J.: Ensemble optimal interpolation schemes for assimilating Argo profiles into a hybrid coordinate ocean model, Ocean Modelling, 33, 283-298, 10.1016/j.ocemod.2010.03.002, 2010b.

Yadav, R., Sugha, A., Bhatti, M. S., Kansal, S. K., Sharma, S. K., and Mandal, T. K.: The role of particulate matter in reduced visibility and anionic composition of winter fog: a case study for Amritsar city, RSC Advances, 12, 11104-11112, 10.1039/D2RA00424K, 2022.

Ye, H., Pan, X., You, W., Zhu, X., Zang, Z., Wang, D., Zhang, X., Hu, Y., and Jin, S.: Impact of CALIPSO profile data assimilation on 3-D aerosol improvement in a size-resolved aerosol model, Atmospheric Research, 264, 105877, https://doi.org/10.1016/j.atmosres.2021.105877, 2021.

Yu, X., Ma, J., An, J., Yuan, L., Zhu, B., Liu, D., Wang, J., Yang, Y., and Cui, H.: Impacts of meteorological condition and aerosol chemical compositions on visibility impairment in Nanjing, China, Journal of Cleaner Production, 131, 112-120, https://doi.org/10.1016/j.jclepro.2016.05.067, 2016.

Zhai, S., An, X., Zhao, T., Sun, Z., Wang, W., Hou, Q., Guo, Z., and Wang, C.: Detection of critical PM2.5 emission sources and their contributions to a heavy haze episode in Beijing, China, using an adjoint model, Atmos. Chem. Phys., 18, 6241-6258, 10.5194/acp-18-6241-2018, 2018.

Zhang, F., Zhang, M., Huang, X.-Y., and Zhang, X.: Intercomparison of an Ensemble Kalman Filter with Three- and Four-Dimensional Variational Data Assimilation Methods in a Limited-Area Model over the Month of June 2003, Monthly Weather Review, 139, 566-572, 10.1175/2010mwr3610.1, 2011.

Zhang, W., Zhang, X., and Wang, H.: The Role of Aerosol-Radiation Interaction in the Meteorology Prediction at the Weather Scale in the Numerical Weather Prediction Model, Geophysical Research Letters, 49, e2021GL097026, https://doi.org/10.1029/2021GL097026, 2022.

Zheng, B., Zhang, Q., Zhang, Y., He, K. B., Wang, K., Zheng, G. J., Duan, F. K., Ma, Y. L., and Kimoto, T.: Heterogeneous chemistry: a mechanism missing in current models to explain secondary inorganic aerosol formation during the January 2013 haze episode in North China, Atmospheric Chemistry and Physics, 15, 2031-2049, 10.5194/acp-15-2031-2015, 2015.

Zheng, H., Liu, J., Tang, X., Wang, Z., Wu, H., Yan, P., and Wang, W.: Improvement of the Real-time PM2.5 Forecast over the Beijing-Tianjin-Hebei Region using an Optimal Interpolation Data Assimilation Method, Aerosol and Air Quality Research, 18, 1305-1316, 10.4209/aaqr.2017.11.0522, 2018.

Zhou, C.-H., Gong, S., Zhang, X.-Y., Liu, H.-L., Xue, M., Cao, G.-L., An, X.-Q., Che, H.-Z., Zhang, Y.-M., and Niu, T.: Towards the improvements of simulating the chemical and optical properties of Chinese aerosols using an online coupled model – CUACE/Aero, Tellus B: Chemical and Physical Meteorology, 64, 18965, 10.3402/tellusb.v64i0.18965, 2012.

https://doi.org/10.5194/gmd-2022-207
Preprint. Discussion started: 7 November 2022

Geoscientific Model Development Discussions

Table1. Experimental design.

Name	Experiment	Design
Control experiment	CR00	Warm restart (WS) at 0000 UTC and without DA
	CR12	WS at 1200 UTC and without DA
Sensitivity experiment	L20km N48 WS00 L40km N48 WS00 L60km N48 WS00 L80km N48 WS00 L100km N48 WS00	Fixed ensemble size N of 48, assimilation of the initial field at 0000 UTC per day, and localization length-scale L of 20, 40, 60, 80, 100 km were selected for the assimilation experiment
	L80km N24 WS 00 L80km N48 WS 00 L80km N72 WS 00 L80km N96 WS 00 L80km N120 WS 00 L80km N144 WS 00	Fixed localization length-scale L of 80 km, assimilation of the initial field at 0000 UTC per day, and ensemble size N of 24, 48, 72, 96, 120, 144 km were selected for the assimilation experiment
Cycling assimilation experiment	DA00	WS at 0000 UTC and with DA
	DA12	WS at 1200 UTC and with DA

585

Table2. Statistics of the analysis fields $PM_{2.5}$ concentrations from 15 to 23 November 2016 at 0000 UTC for the sensitivity experiments with localization length-scale of 80km and ensemble size N of 24, 48, 72, 96, 120,144

	24	**48**	**72**	**96**	**120**	**144**
CORR	0.970	0.974	0.975	0.975	0.959	0.961
RMSE (ug m-3)	20.675	19.170	18.908	18.849	23.919	23.416
MB (ug m-3)	2.160	1.963	1.943	1.938	2.514	2.560
ME (ug m-3)	12.061	11.158	10.943	10.858	13.997	13.532

https://doi.org/10.5194/gmd-2022-207
Preprint. Discussion started: 7 November 2022

Geoscientific Model Development Discussions

590

Table 3. Statistical comparison of $PM_{2.5}$ concentrations from the BFs and the assimilation experiment with 96 ensemble samples and a length-scale of 40km (AFs) with all observations analyses by 0000UTC during the experiment period. The Total is China Mainland. The NC is North China.

		CORR	RMSE	MB	ME
Total	**BF**	0.584	62.449	-0.416	41.578
	AF	0.967	17.280	2.137	10.174
	/	65.58%	-72.33%	-628.16%	-75.53%
NC	**BF**	0.391	98.639	-21.287	71.941
	AF	0.972	23.149	2.050	15.870
	/	148.59%	-75.53%	-109.63%	-79.59%

595

https://doi.org/10.5194/gmd-2022-207
Preprint. Discussion started: 7 November 2022

Geoscientific Model Development Discussions

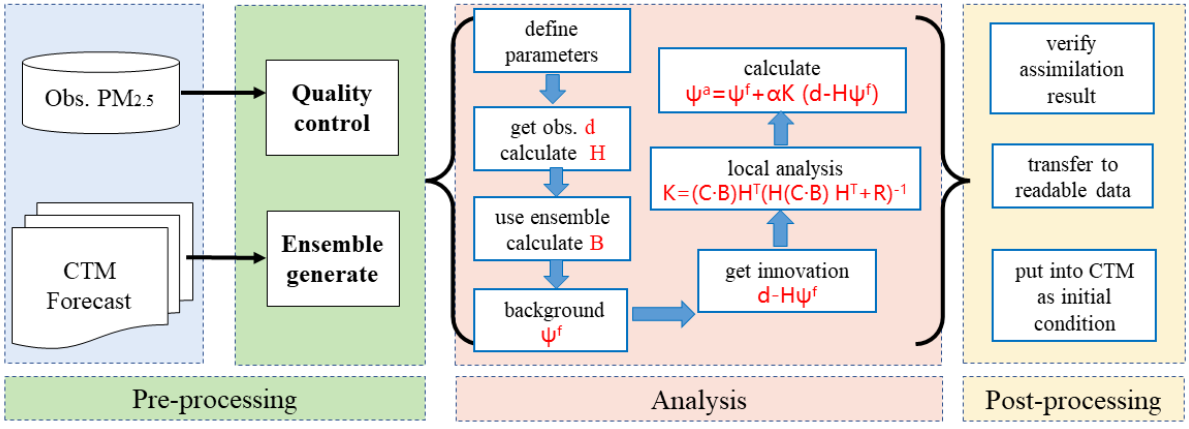

Figure 1. Flow chart of the main calculation procedures for EnOI initial field assimilation. The Obs. $PM_{2.5}$ is ground-based observation of $PM_{2.5}$. The CTM is chemistry transport model.

600

https://doi.org/10.5194/gmd-2022-207
Preprint. Discussion started: 7 November 2022

Geoscientific Model Development Discussions

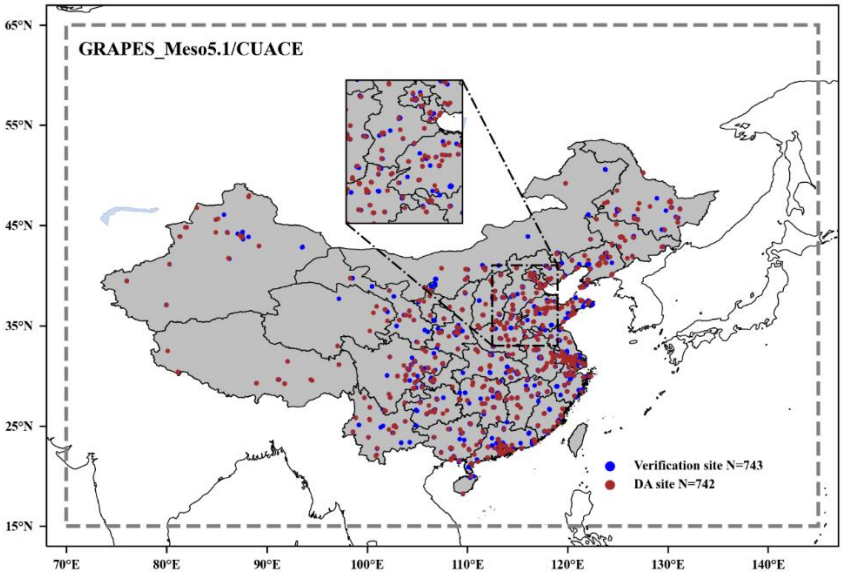

Figure 2. Simulation domain of GRAPES_Meso5.1/CUACE. Minor region represents North China (NC). The locations of ground stations in China mainland are marked on the maps with blue and brown dots. Only when the independence test is performed, the brown assimilation sites and the blue verification sites are distinguished, otherwise, all sites are used as assimilation sites.

https://doi.org/10.5194/gmd-2022-207
Preprint. Discussion started: 7 November 2022

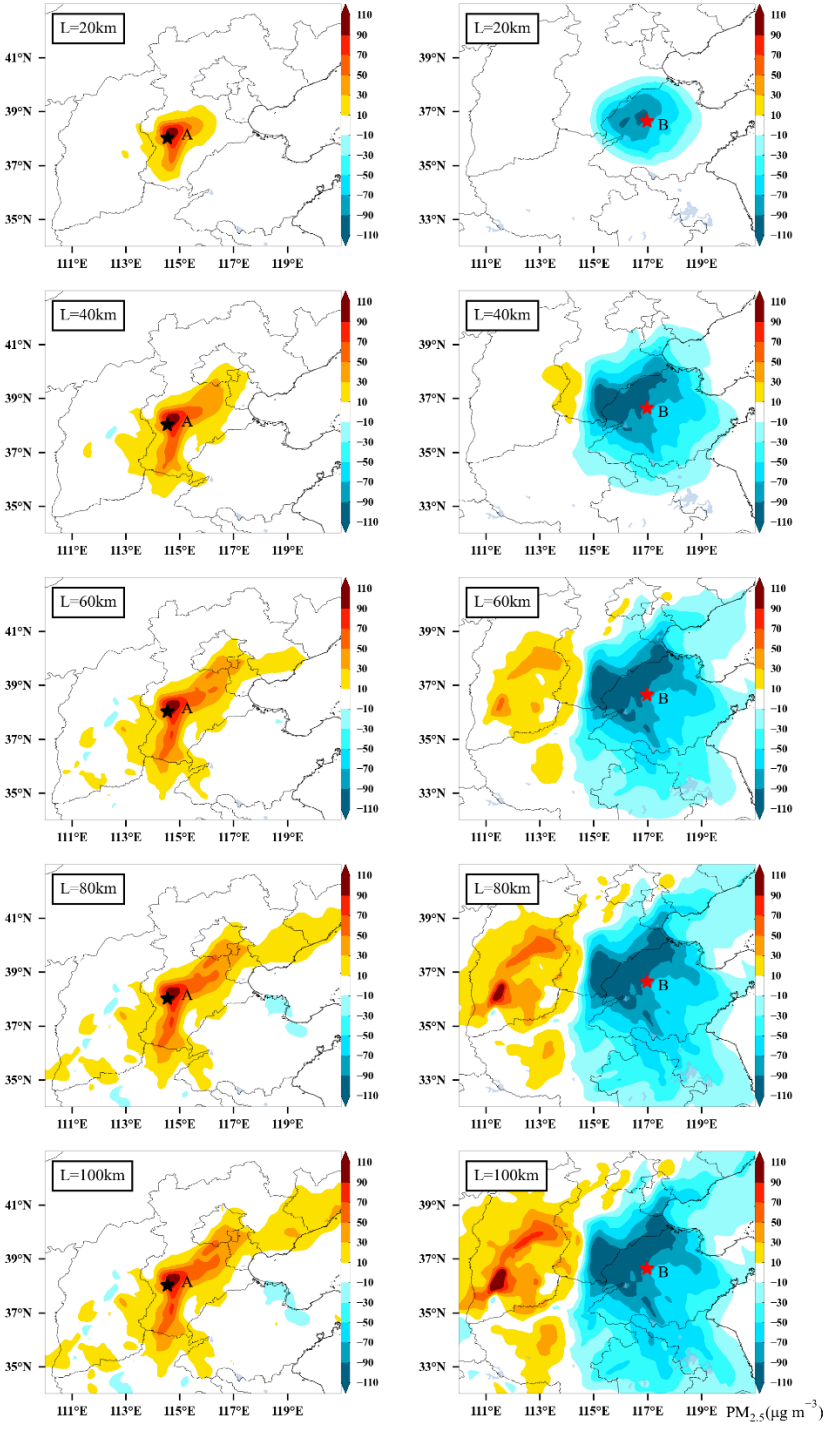

Figure 3. Spatial distribution of $PM_{2.5}$ analysis increments after assimilation of initial fields at 0000 UTC on 15 December 2016, for assimilation site A (38.0° N, 114.5° E) only (left column) and assimilation site B (36.6° N, 116.9° E) only (right column) with fixed ensemble size 48 and different localization length-scale of 20, 40, 60, 80, 100km.

https://doi.org/10.5194/gmd-2022-207
Preprint. Discussion started: 7 November 2022

Geoscientific Model Development Discussions

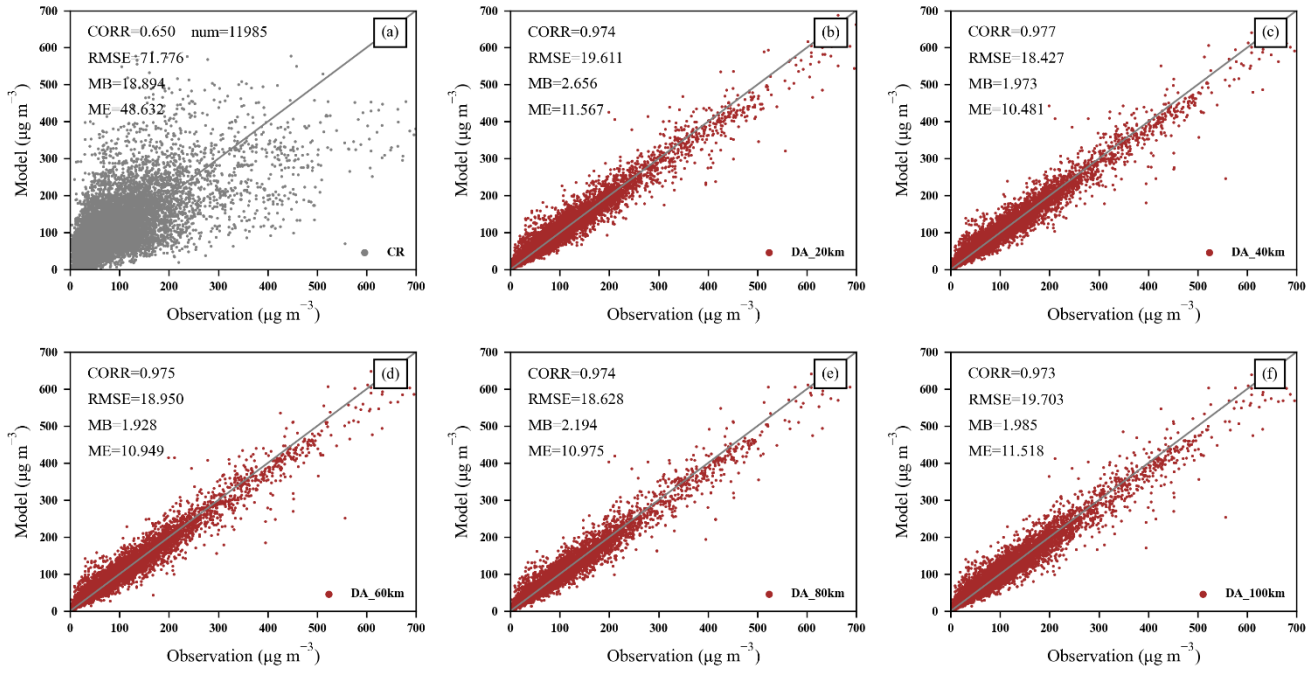

Figure 4. Scatter plot of $PM_{2.5}$ concentrations from the control experiment (CR) and the assimilation experiment with 40 ensemble samples and length-scale L of 20, 40, 60, 80, 100km (DA) with all observations analyses by 0000UTC during the experiment period. The num is the sum of all ground-based observations of $PM_{2.5}$ stations during the experiment period.

615

https://doi.org/10.5194/gmd-2022-207
Preprint. Discussion started: 7 November 2022

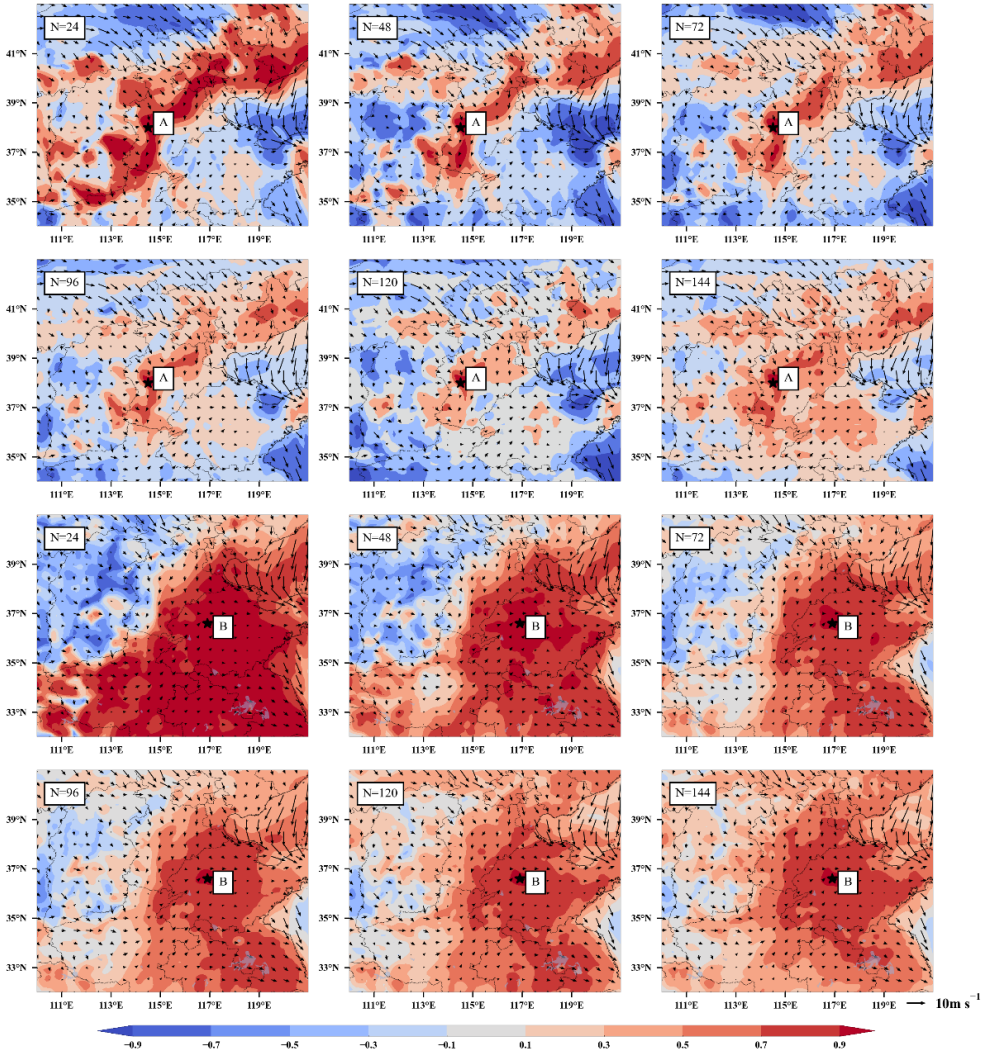

Figure 5. Spatial distribution of correlation coefficients for site A (38.0° N, 114.5° E) (rows 1, 2) and site B (36.6° N, 116.9° E) (rows 3, 4) with ensemble error for assimilation experiments using length-scale of 80km and different ensemble size N of 24, 48, 72, 96, 120, 144 and wind vectors at 0000 UTC on 15 December 2016.

620

https://doi.org/10.5194/gmd-2022-207
Preprint. Discussion started: 7 November 2022

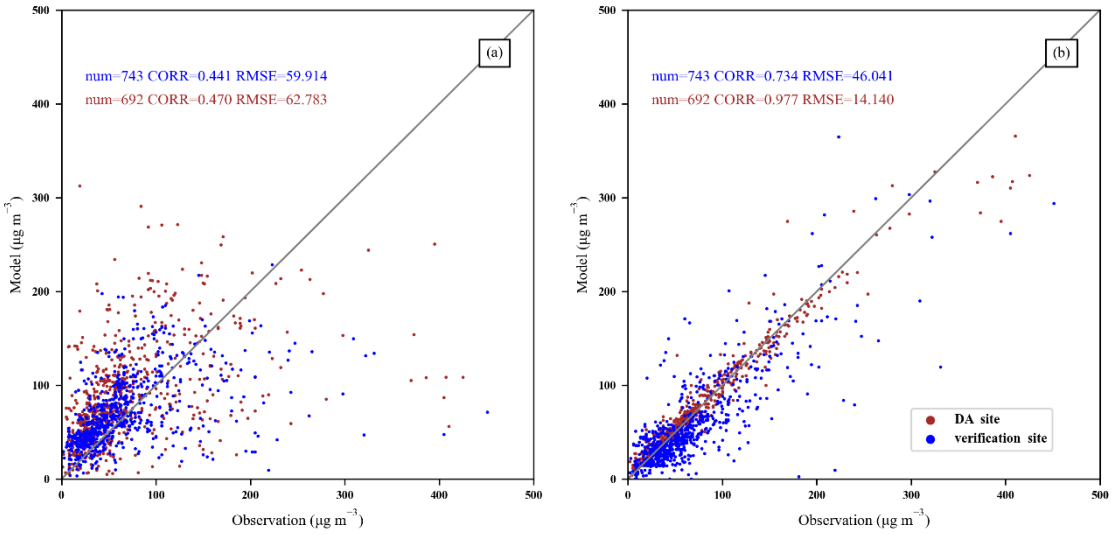

Figure 6. Scatter plot of $PM_{2.5}$ verification sites compared to assimilation (DA) sites for the control experiment (a) and assimilation experiment (b) using length-scale L=40km and ensemble size N=96 at 0000UTC on 15 December 2016.

https://doi.org/10.5194/gmd-2022-207
Preprint. Discussion started: 7 November 2022

Geoscientific Model Development Discussions

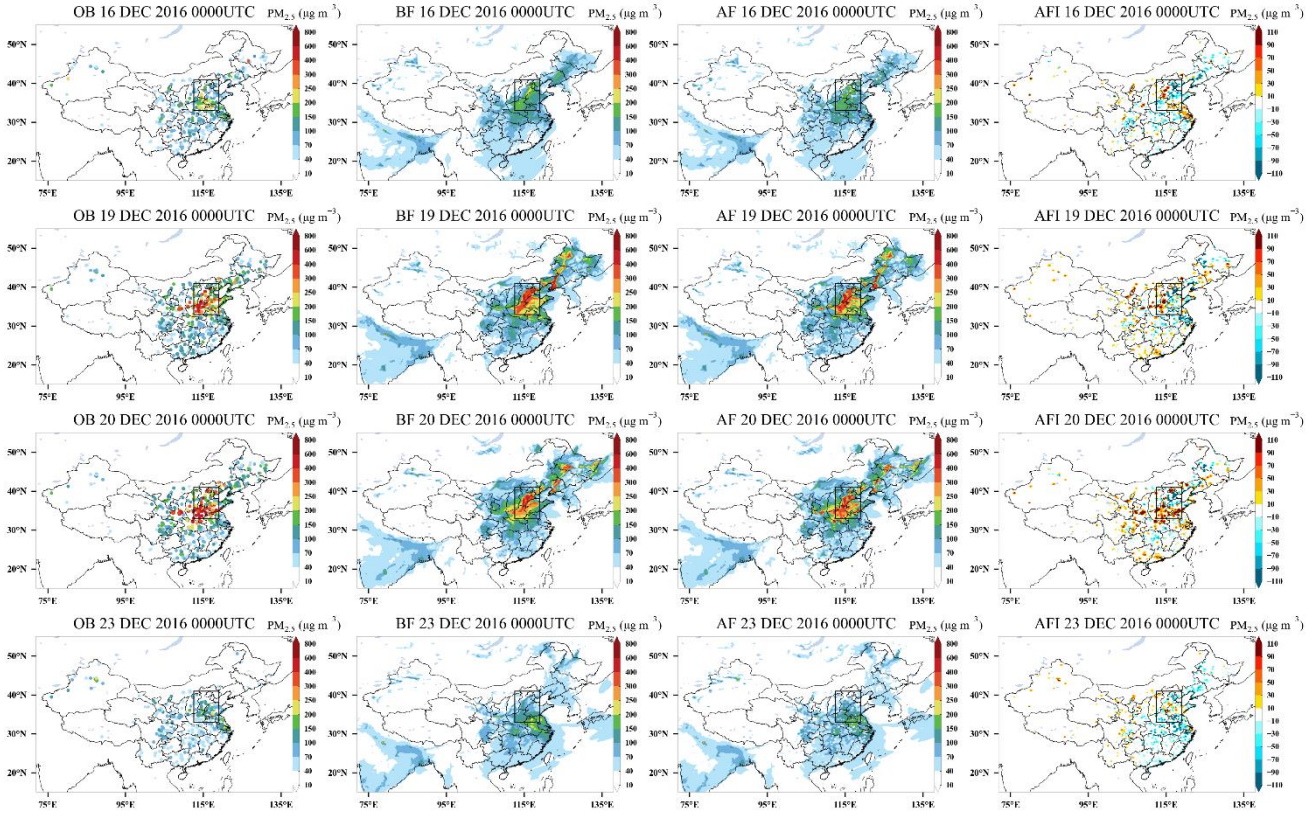

625

Figure 7. Snapshots of the horizontal distributions of $PM_{2.5}$ observation (OB), before (BF) and after (AF) the application of EnOI technique, analysis field increment (AFI) at 0000 UTC on 16, 19, 20, and 23, December 2016. The black box area, representing northern China (NC), has the most serious $PM_{2.5}$ pollution.

https://doi.org/10.5194/gmd-2022-207
Preprint. Discussion started: 7 November 2022

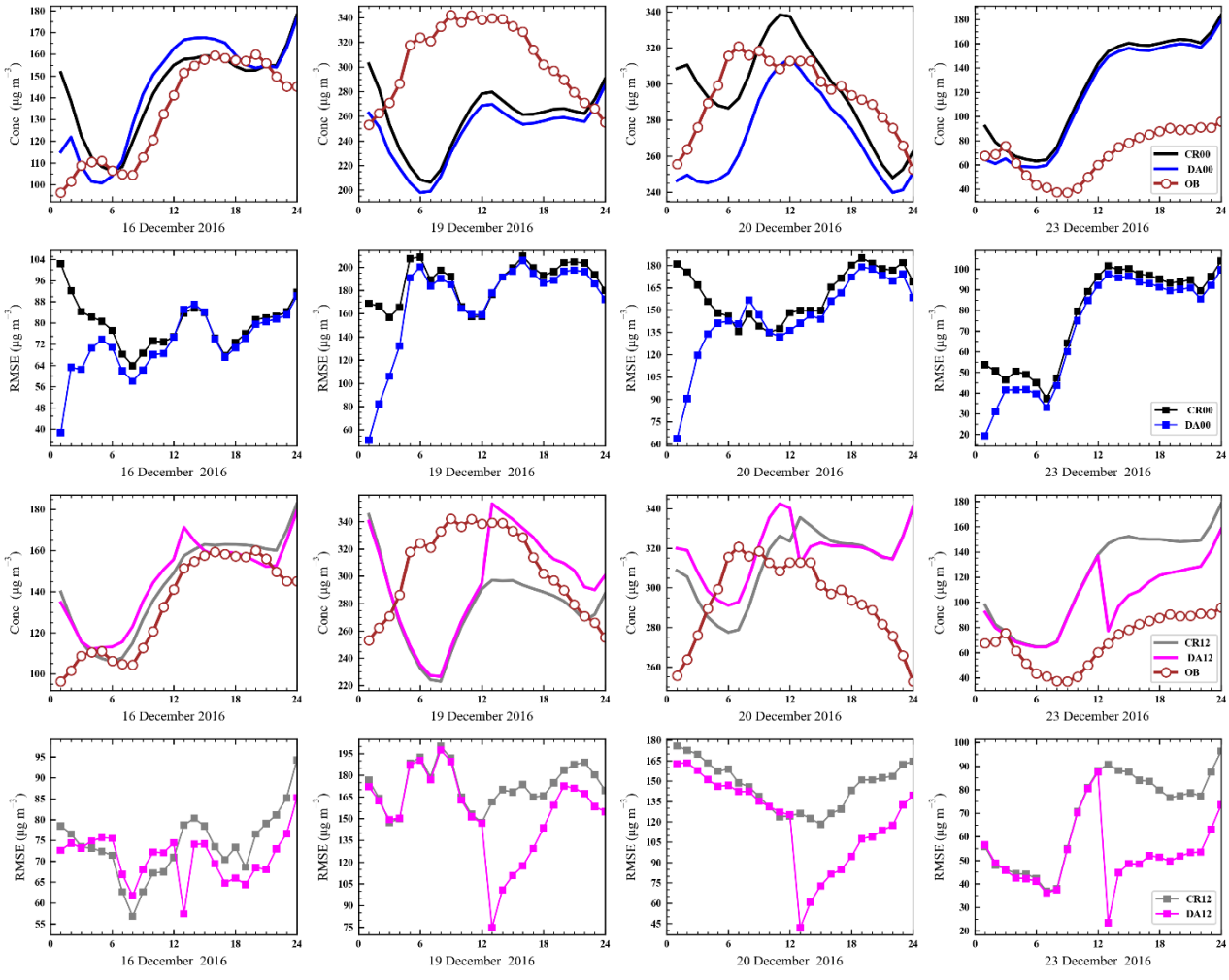

630 **Figure 8. Mean forecasts and observations of $PM_{2.5}$, RMSE for North China, calculated against observations. x-axis refers to specific dates. The labels on the x-axis refer to the 24 hours of the day. DA00 and DA12 represent the initial field assimilation using EnOI at 0000 UTC and 1200 UTC each day, respectively. CR00 and CR12 are control experiments, representing warm restart without assimilation at 0000 UTC and 1200 UTC each day. The OB is hourly results of $PM_{2.5}$ observations averaged over the North China region.**

635

https://doi.org/10.5194/gmd-2022-207
Preprint. Discussion started: 7 November 2022

Geoscientific Model Development
Discussions
Open Access
EGU

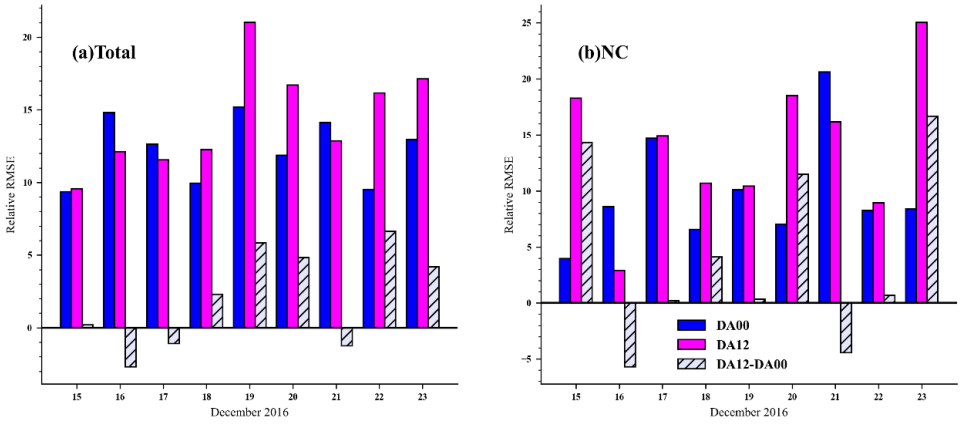

Figure 9. Relative RMSE time series for 15 to 23 December 2016 for Mainland China (a), North China (b). The relative RMSE is calculated by the daily average RMSE.

640

https://doi.org/10.5194/gmd-2022-207
Preprint. Discussion started: 7 November 2022

Geoscientific Model Development Discussions

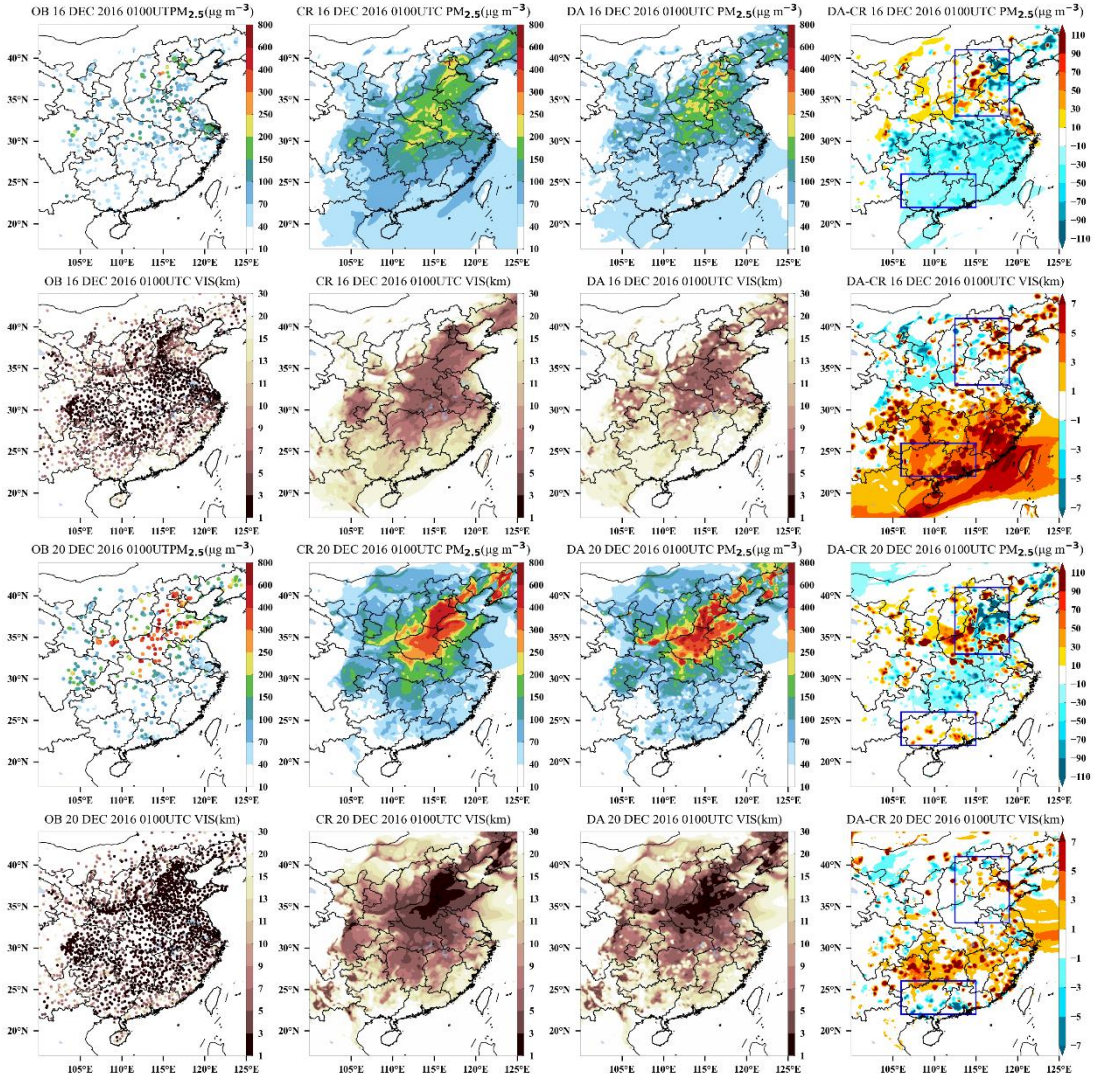

Figure 10. Snapshots of $PM_{2.5}$ and visibility horizontal distribution for control (CR), assimilation (DA), observation (OB), and increment (DA-CR) at 0100 UTC after assimilation of the initial field at 0000 UTC on 16 and 20 December 2016.The upper box represents northern China and the lower box represents Guangxi and Hainan in China.

https://doi.org/10.5194/gmd-2022-207
Preprint. Discussion started: 7 November 2022

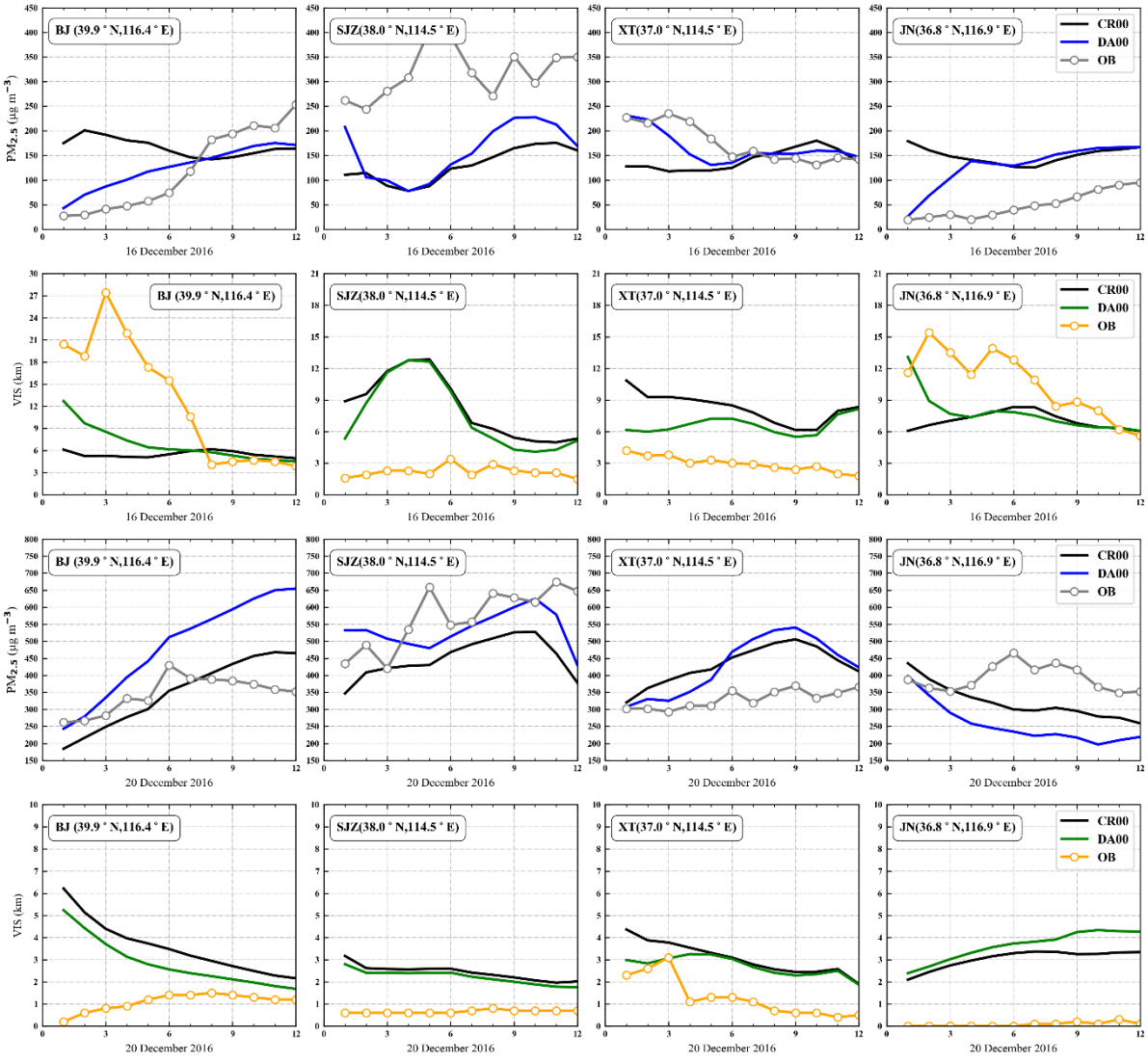

645

Figure 11. Comparison of $PM_{2.5}$ and visibility observations, assimilation experiment simulations (DA00), and control experiment simulations (CR00) after assimilation of the initial field at 0000 UTC each day. Four cities are exemplified, from left to right, Beijing (BJ), Shijiazhuang (SJZ), Xingtai (XT), Jinan (JN). The labels on the x-axis refer to the first 12 hours of 16 and 20 December 2016.